

Synthetic seismic modelling and imaging of an impact structure

Matteo Niccoli

ABSTRACT

A geologic depth and velocity model of an impact crater was created and ray-traced. The resultant seismic data were pre- and post-stack migrated both in depth and time with the objective of evaluating which algorithm best performs in the case of a complex geologic structure, and determine which events are less well imaged. Kirchhoff migration was used in all four cases. Both pre-stack and post-stack depth migrations imaged fault planes well when contrasting lithologies were present either laterally or vertically across the planes. Both depth migrations have also well imaged the upturned layers in the central uplift. The pre-stack depth migration has better imaged deep reflectors; it has also succeeded in imaging events in the most challenging part of the section, below a complex shaped, low velocity breccia deposit. Pre-stack time migration produced superior results in terms of imaging some events, in particular the upturned layers in the central uplift. The migration, however, has performed poorly in the deep section. The post-stack time migration performed very poorly as a result of an insufficient smoothing of the migration velocity field that has affected the imaging and spread across the section. Time to depth conversion is recommended to evaluate the positioning of migrated events.

INTRODUCTION

Of the more than 150 impact craters currently known, approximately 25% have been associated with economic deposits, and 17 are currently being actively exploited (Grieve and Masaytis, 1994). Brown (2002) highlighted the two most interesting aspects about the petroleum potential of impact craters: 1) mixed breccia deposits are formed during the impact that make excellent reservoirs; 2) more than one part of the impact structure can host hydrocarbon accumulations. Mazur and Stewart (1997) provide an excellent review of impact structures currently investigated by the Applied Geophysics Group at the University of Calgary. In addition to its significance for the entire scientific community, crater research is aimed at extending the current knowledge about impact structure hydrocarbon potential.

Kirtland Grech et al. (1998), performed a modeling experiment of a thrust model with a complex velocity structure, and compared a number of pre-stack and post-stack migration algorithms. The authors discussed the performance of each algorithm in positioning and focussing a number of events that are typical of thrust environments. More recently, Isaac and Lines (2002) have compared the performance of pre-stack depth migration as opposed to pre-stack time migration. They used synthetic seismic data created by ray-tracing a depth model with vertical and lateral velocity variations, and have shown that time migration in some cases does not position accurately events, even when the exact velocity field is used.

In this work I built a geologic depth and velocity model of a complex crater structure, ray-traced the model, and then pre-stack and post-stack migrated the synthetic data both in time and depth. The main objective of the work was to examine and compare the

resulting migrated sections and evaluate which algorithm performs best in the case of a crater structure, and also to determine which events are less well imaged, if any.

SYNTHETIC MODELLING

Geologic model

The features of interest in a complex crater are summarized in Figure 1, including normal faults and slumped blocks in the rim, breccia deposits, and a well-developed central peak with upturned layers. Figure 3 shows an example interpreted seismic line across the Hotchkiss structure (Mazur et al., 1999).

The geological model used in this work is shown in Figure 3 and comprises all the summarized features present in real complex craters. The structure was buried under a cover of sands that to provides a flat surface for sources and receivers during ray tracing. The surface also served as a ~flat datum during data processing. That way, no static corrections and velocity field manipulations were needed.

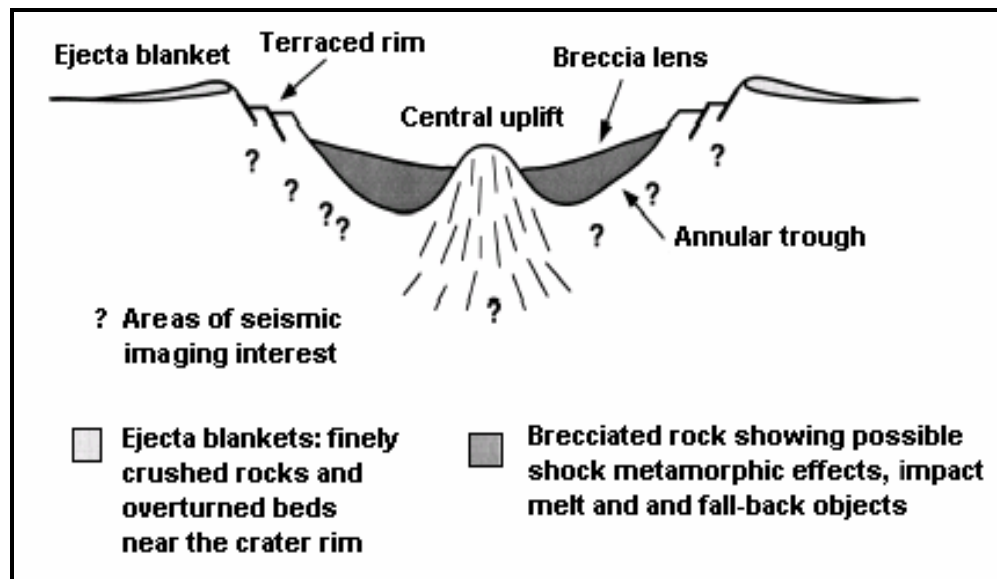


FIG. 1. Schematic of a complex crater (Westbroek and Stewart, 1995).

GXII ray tracing and trace generation

The ray tracing was carried out in GX II with a Common Source simulation. A split spread geometry was chosen, with both a shot interval and receiver separation of 50 m, for the total length of the section (5000 m). To generate the traces, data have then been sorted into panels of rays for each individual shot and convolved with a Ricker wavelet 256 ms long and with dominant frequency of 30 Hz. The traces were 3500 ms long, with a sampling interval of 2 ms. Geometrical spreading and seismic attenuation were not included in the generation process.

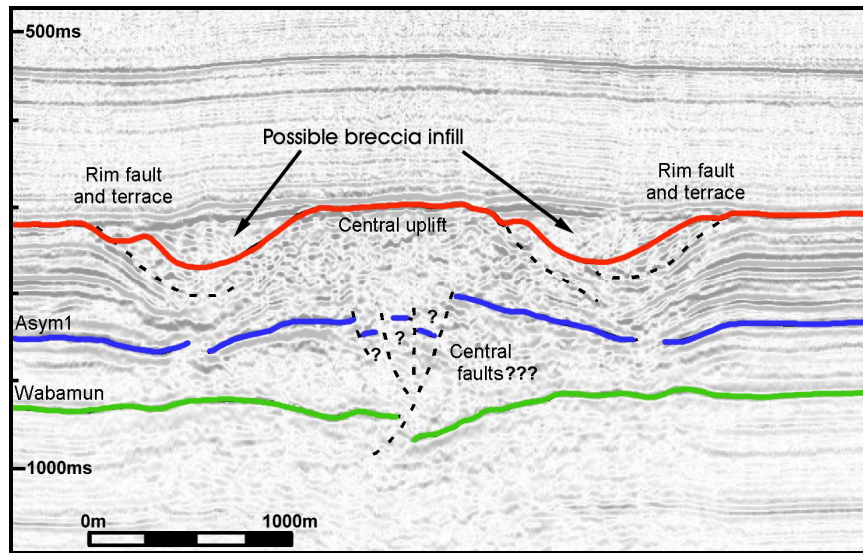


FIG. 2. Interpreted seismic section over the Hotchkiss structure of Alberta (Mazur et al., 2000).

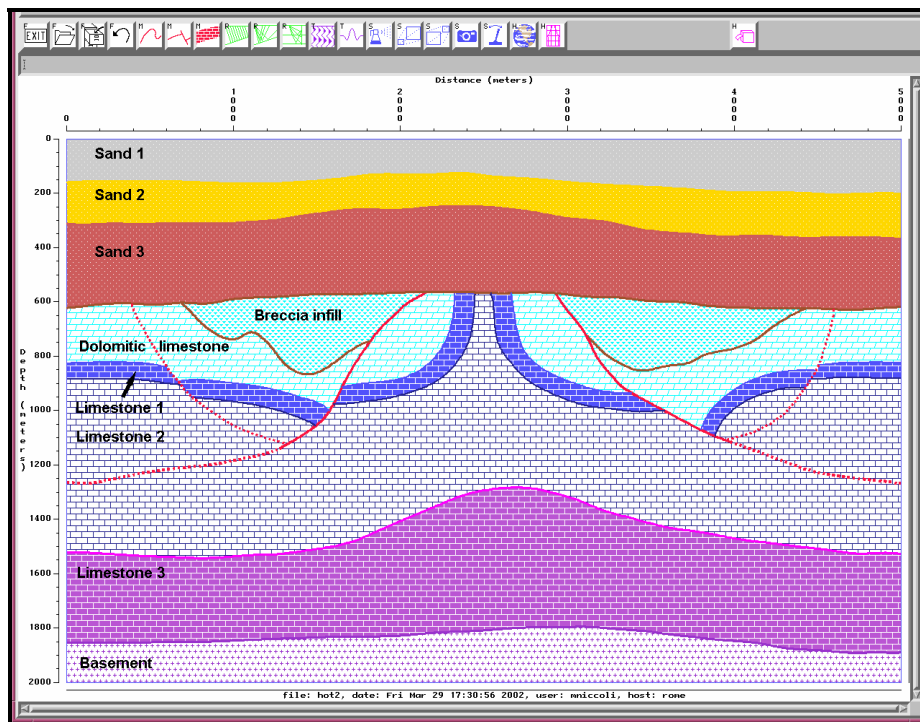


FIG. 3. Geologic model built in GX II. The velocity model is plotted in Figure 5 and summarized in Table 2.

Processing in Promax

Shot gathers were exported in Promax as IBM SEG Y files for further processing and migration as summarized in Table I. An example GXII trace panel is shown in Figure 4 along with the corresponding Promax shot gather.

Table I. Promax processing flow.

Pre-stack processing flows		Post-stack processing flows	
Time	Depth	Time	Depth
AGC	AGC	AGC	AGC
Kirchhoff migration	Kirchhoff migration	NMO	NMO
Stack	Stack	DMO	DMO
		Stack	Stack
		Kirchhoff migration	Kirchhoff migration

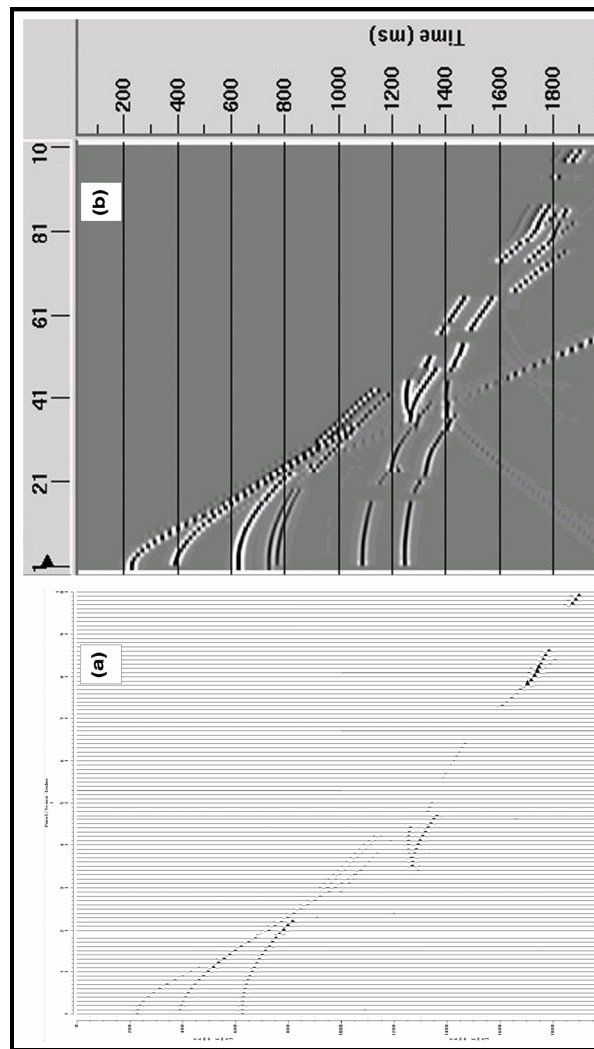


FIG. 4. a) Example GXII trace panel; b) example Promax shot gather. Notice the reflection gaps in the shot gather due to the structure-induced ray bending.

All migrations used the Kirchhoff algorithm, with a CDP interval of 25 m and maximum frequency of 80 Hz. The maximum dip allowed to migrate was 80 degrees. The interval velocity model is shown in Figure 5 and also summarized in Tab. II. This model was exported from GXII to Grid2pro and reformatted for use in Promax, where it was used to create the RMS velocity model for migration.

RESULTS AND CONCLUSIONS

Because the model is structurally complex, both the pre-stack and post-stack migrations were performed using a Kirchhoff algorithm. This migration is described (Promax reference manual, 1995, and Kirtland et al., 1998), as a reasonable algorithm in this kind of geological environment, for its ability to handle both steep dips and laterally varying velocities.

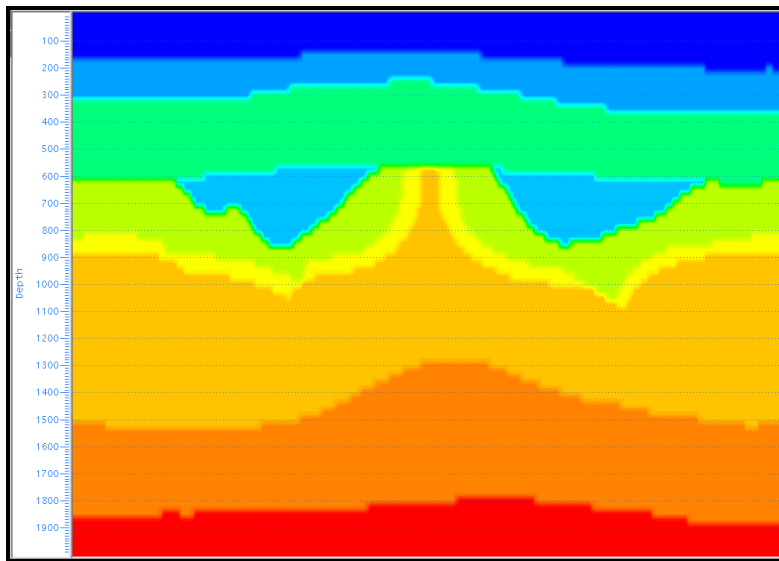


FIG. 5. Interval velocity model used to generate the synthetic seismic traces. The velocities are summarized in Table 2.

Table 2. The velocity model used in the generation of the synthetic seismic section.

Formation	Velocity (m/s)
Sand 1	1400
Sand 2	1900
Sand 3	2600
Dolomitic limestone	3600
Breccia infill	2000
Limestone 1	3800
Limestone 2	4000
Limestone 3	4200
Basement (granite)	4600

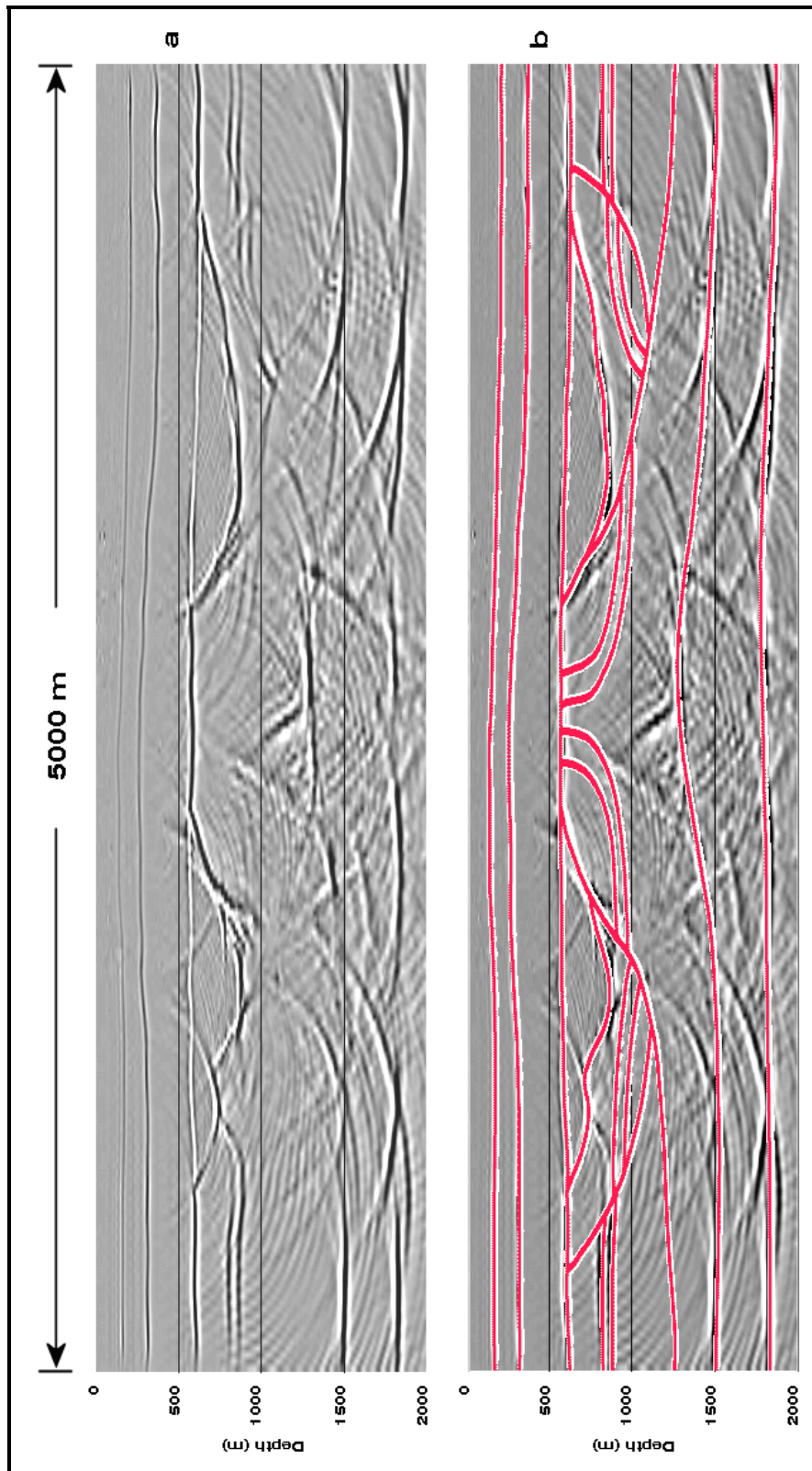


FIG. 6. a) Post-stack depth migrated section; b) migrated section with superimposed geological model; horizontal exaggeration 1.75.

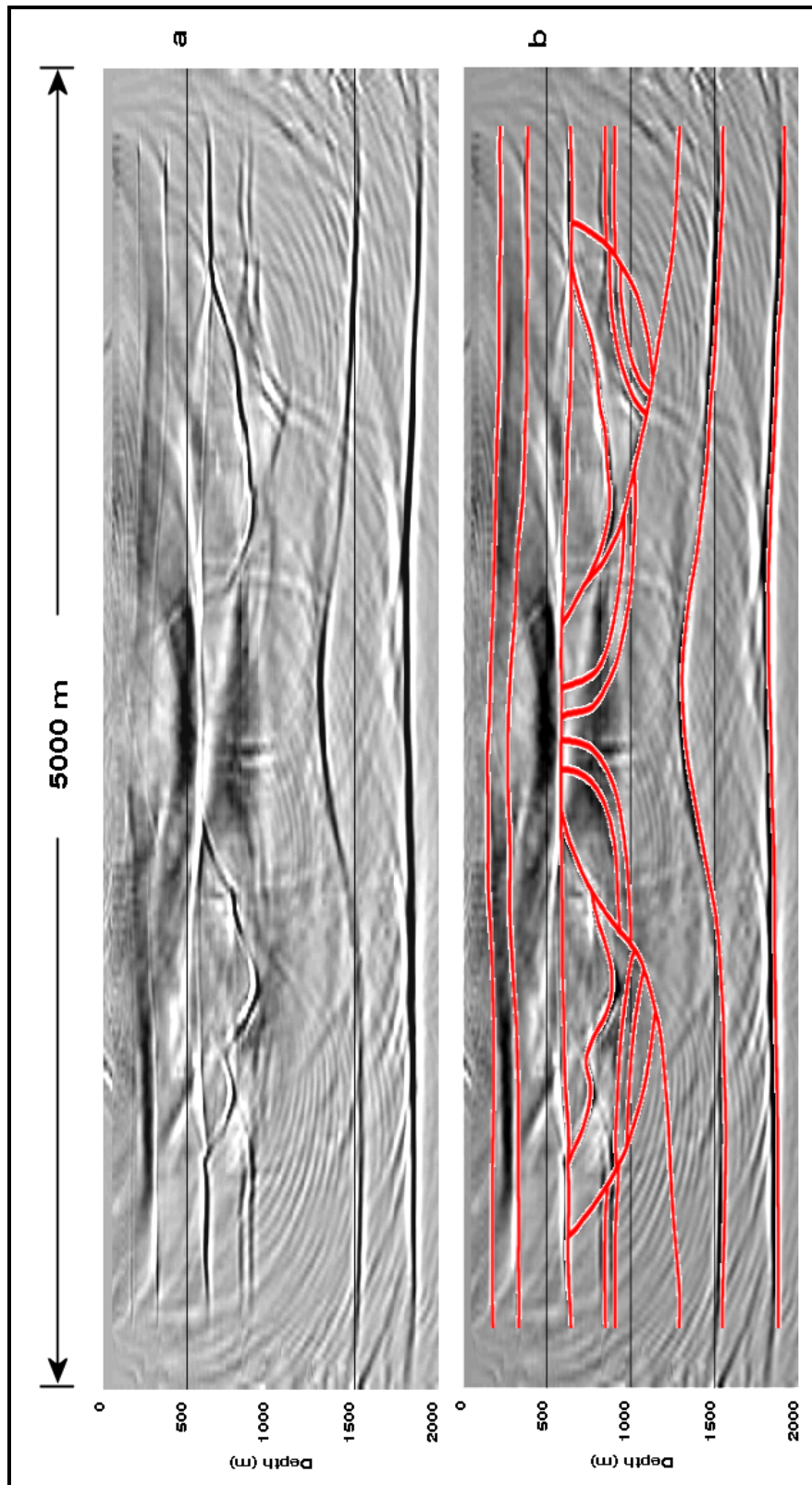


FIG. 7. a) Pre-stack depth migrated section; b) migrated section with a superimposed geological model; horizontal exaggeration 1.75.

Figure 6 and 7 show the two final depth migrations, post-stack and pre-stack, respectively. The geological model is superimposed to the migrated sections in Figure 6b and Figure 7b. The most important results are summarized in Figures 8, 9, and 10, and discussed below.

Shallow section

The pre-stack depth migration (Figure 8a) performed poorly in the shallow section. On the contrary, the post-stack migration perfectly imaged the top of sand 2 and top of sand 3, indicated respectively by cyan and black arrows in both figures.

Upturned, steep layers

Both depth migrations imaged relatively well the upturned layers of limestone 1 within the central peak (yellow arrows in Figure 8) The post-stack section (Figure 8a) gave a slightly superior result for the steep most part of the layers. These results confirms the ability of the Kirchhoff migration algorithm to handle steep dips. (Consider that in both cases the maximum dip to migrate was 80 degrees).

Deep section

The pre-stack migration (Figure 8b) imaged very well the top of limestone 3 and the top of the basement, indicated respectively by red and green arrows in both figures. These events are also imaged at their correct position in the post-stack migrated section (Figure 8a), although the section is a lot noisier and has spread migration smiles.

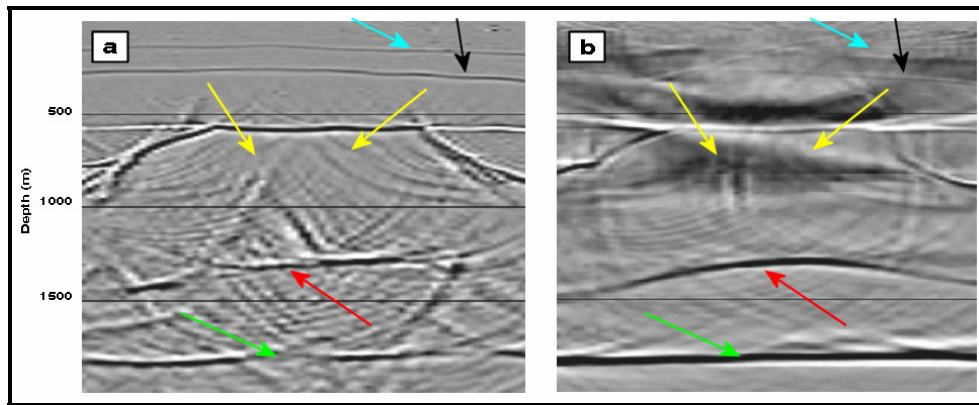


FIG. 8. Comparison of results for the shallow events, upturned layers, and deep events in a) post-stack depth migration, and b) pre-stack depth migration. The cyan arrow indicates top of sand 2, the black arrow top of sand 3; The upturned strata are indicated by yellow arrows; top of limestone 3 and basement are indicated by a red and green arrow, respectively. Both migrations have performed very well in terms of positioning. The pre-stack migration has worked better in terms of focussing of events in the intermediate and deep section. The post-stack migration, though with a much noisier appearance, has better imaged the shallow events and the steep most portion of the upturned layers.

Sub-breccia events and fault planes

Figure 9 shows the results for the right-hand side of the model and Figure 10 those for the left-hand side. The fault planes are indicated by dotted lines in the two figures. A number of events were less well imaged, some parts of the fault planes in particular.

However, the poor results must not be attributed to failure of the migration algorithms; it is due in most cases to the absence of acoustic impedance across part of the interfaces, where the same lithology is present in both the footwall and the hanging wall. On the other hand, where a contrasting lithology is present either laterally or vertically, the planes are well imaged, as at the locations indicated by white and cyan arrows in Figure 9, and green and black arrows in Figure 10, respectively.

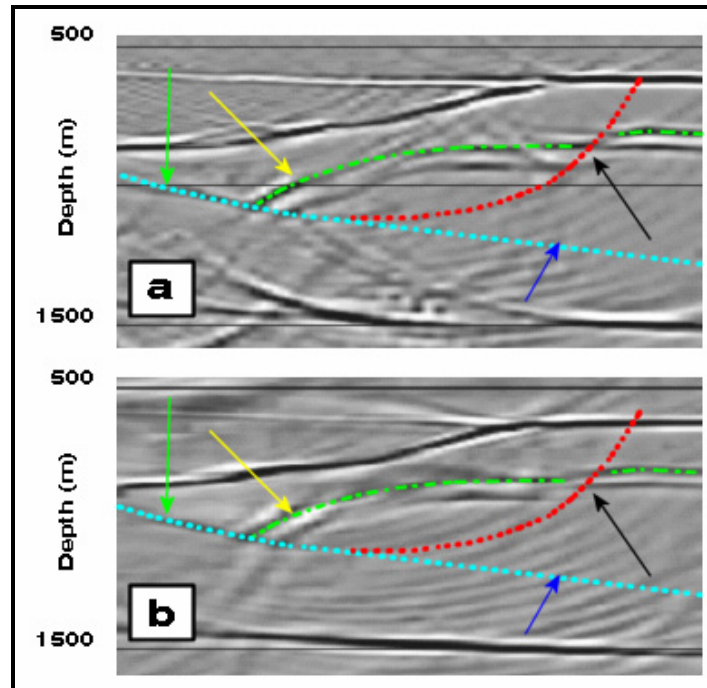


FIG. 9. Comparison of results for the right side sub-breccia events and fault planes in a) post-stack depth migration, and b) pre-stack depth migration. The dotted red and cyan lines indicate fault planes; the green dash-dot line indicates the top of limestone 1. Both algorithms have imaged the top of this formation at the correct depth, even underneath the low velocity breccia (yellow arrows). The fault planes are not imaged at all except at the two locations where a lithology contrast exists: 1) the displaced top of limestone 1, indicated by black arrow; and 2) the transition from dolomitic limestone to limestone, indicated by green arrow (compare to the fault plane at location indicated by the blue arrow, where no lithology contrast is present).

The orange arrows in Figure 9 indicate the area where the pre-stack migration performed better than the post-stack migration, that is in imaging the displaced top of limestone 1 (dash dotted green line) below the left-hand side breccia deposit. To this regard, the shape of the low velocity deposits may play an important role. Indeed, both migration algorithms performed well in imaging the top of limestone 1 below the right-hand side breccia deposit (yellow arrows in Figure 10), where the deposit itself had a more simple shape. This result suggests that a structurally complex lateral variation in velocity can affect migration results, although pre-stack migration seems to handle it better than post-stack migration (compare orange arrows in Figure 9a and 9b).

Post-stack TIME versus post-stack DEPTH migration

Figure 11 displays a post-stack time migrated section. Compared to the post-stack depth section, some events are better focused, in particular the upturned limestone 1 layers

within the central peak (green arrows). The time migration, however, has performed poorly in the deep section (red ellipse).

Pre-stack TIME migration

Pre-stack time migration was also attempted. The resulting section is plotted in Fig. 12. Most of the events display an unattractive step-like character. This unpredicted result is due to the step-like character of the shallow interfaces in the velocity model. Figure 13 shows the upper ~1100 ms of the RMS velocity field. By comparison of Figure 13 with the upper portion of the interval velocity model in Figure 5, it is evident that the RMS velocity field is significantly smoothed on the vertical direction. However, smoothing failed to remove the step-like character. This affected not just the imaging of the shallow reflectors in the final migration, but spread across the entire section.

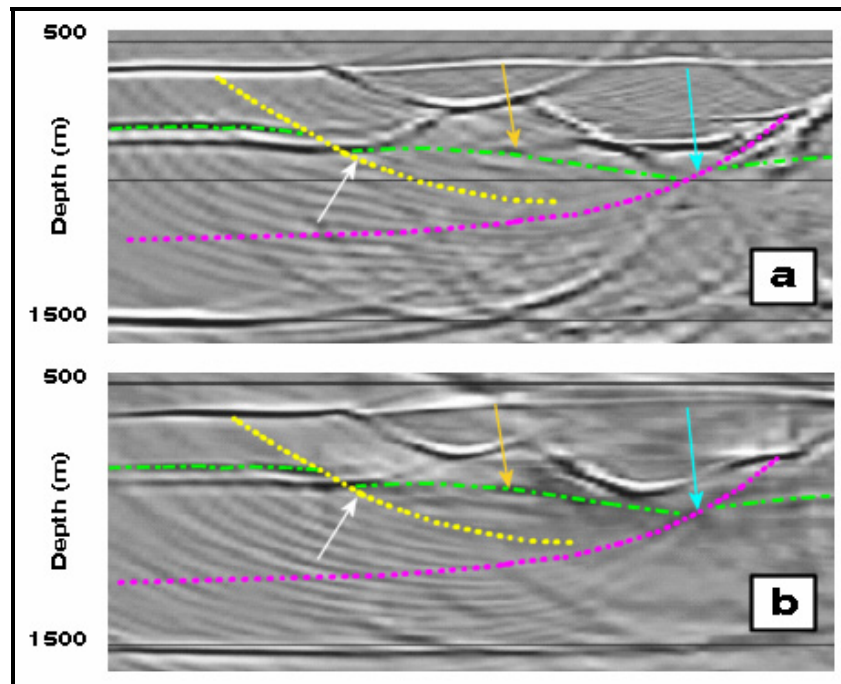


FIG. 10. Comparison of results for the left side sub-breccia events and fault planes in a) post-stack depth migration, and b) pre-stack depth migration. The dotted yellow and magenta lines indicate fault planes; the green dash-dot line indicates the top of limestone 1. Both algorithms have imaged the fault planes only at the two locations where top of limestone 1 is dislocated and a lithology contrast exists (indicated by white and cyan arrow); the orange arrows indicate the area where the pre-stack migration performed better than the post-stack migration, that is in imaging the displaced top of limestone 1 below the complexly shaped, low velocity breccia deposit.

FUTURE WORK

Ray tracing and pre-stack TIME migrating with a smoothed velocity model

Pre-stack time migration was also tested in Promax, as anticipated in Tab. II. The resulting section is plotted in Fig. 11. Most of the events display an unattractive step-like character. This unpredicted result is due to the step-like character of the shallow interfaces in the velocity model. Fig. 11 shows the upper ~1100 ms of the RMS velocity

field. By comparison of Fig. 11 with the upper portion of Fig. 6, it is evident that the RMS velocity field is significantly smoothed on the vertical direction. However, smoothing failed to remove the step-like character. This not only affected the imaging of the shallow reflectors in the final migration. Indeed, it spread across the entire section. Therefore, a new, smoothed velocity model will be used to perform both ray tracing in GX II, and pre-stack time migration in Promax.

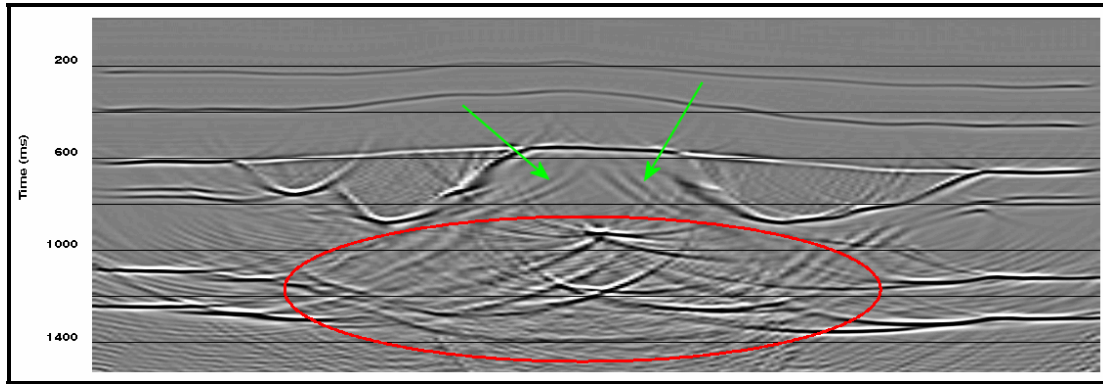


FIG. 11. Post-stack TIME migration. The algorithm has imaged successfully the upturned, steep layers, shallow reflectors and breccia deposits, but performed very poorly in the deep section.

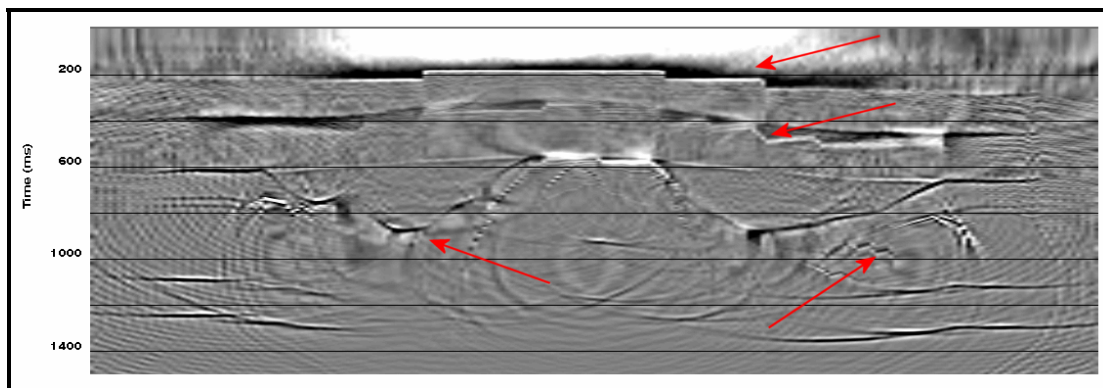


FIG. 12. Pre-stack TIME migration. Notice how the poorly smoothed, step-like character in the shallower RMS velocity transition (Figure 13) has affected the imaging and spread across the section (as indicated by the red arrows).

Time migration with velocity model from conventional velocity analysis

Additional work should also include migrating and comparing the performance of each algorithm when migration velocity is derived from conventional velocity analysis rather than from the exact interval velocity field.

Testing the time migrations positioning accuracy: GX II time to depth conversion

The GX II software offers a possibility to further investigate the problem by testing the time migration. The program provides a feature that allows a time to depth conversion. The procedure is described in the GX II Training Manual, and can be summarized as follows: 1) traces from a seismic section can be imported into GX II and can be used as a “backdrop” for model building, with the model automatically calibrated

on a time scale, which GX II derives from the imported data; 2) the Layer Migration tool can migrate, through an image-ray conversion, the time section to a depth section; 3) this final depth section can be compared to the depth migrated section generated in Promax.

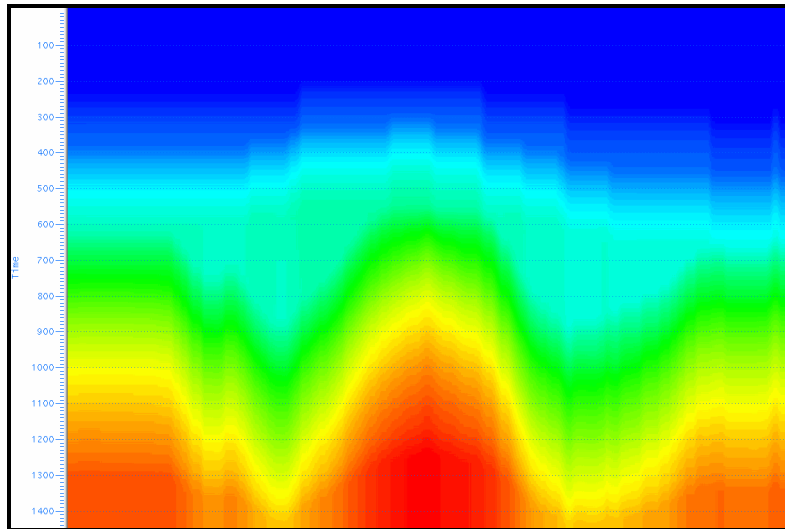


FIG. 13. RMS velocity model used for migration.

ACKNOWLEDGEMENTS

I wish to thank Shauna Oppert, former CREWES student, for sharing with me her Promax bag of tricks, hence contributing greatly to this study. I am indebted to John Bancroft for the many insightful lectures on migration and modelling of seismic data and for his useful comments during this research. I also thank Alan Hildebrand for teaching me a lot about impact craters. Finally, I thank Rob Stewart for his useful comments and suggestions, and for taking the time to revise this paper.

REFERENCES

- Brown, D., 2002, Meteorites make good impression, AAPG Explorer, March 2002, 36-39.
- Grieve, R.A.F., and Masaytis, V.L., 1994, The economic potential of terrestrial impact craters: Internat. Geol. Rev., **36**, 105-151.
- GX II (release 2.1) Training Manual, 3.1-3.19, GX Technology Corporation, Texas, 1995.
- Hodge, P., 1994, Meteorite craters and impact structures of the Earth, Cambridge University Press.
- Isaacs, J.H., and Lines, L.R., 2002, Where's the reef?: CSEG Recorder, March 2002, 30-32.
- Kirtland Grech, M.G., Lawton, D.C., and Spratt, D.A., 1998, Numerical seismic modeling and imaging of exposed structures: FRP Research Report, **4**, 1.1-1.37.
- Mazur, M.J., and Stewart, R.R., Hildebrand, A.R., Lawton, D.C., and Westbroek, H.H., 1999, Seismic characterization of impact craters: A summary: CREWES Research Report, **11**.
- Mazur, M.J., and Stewart, R.R., 1997, The seismic expression and hydrocarbon potential of meteorite impact craters: current research: CREWES Research Report, **9**, 38.1-38.14.
- Melosh, H.J., 1989, Impact cratering, a geologic process, Oxford monographs on Geology and Geophysics #11.
- Promax Reference Manual Vol. 2, 1995 Advanced Geophysical Corporation, Englewood, CO, 1995.
- Westbroek, H.H., and Stewart, R.R., 1995, Seismic interpretation of the White valley structure: A possible meteorite impact crater: CREWES Research Report, **7**, 19.1-19.18.